

## Hybrid electromagnetic and electrostatic micromachined suspension with adjustable dynamics

This content has been downloaded from IOPscience. Please scroll down to see the full text.

2015 J. Phys.: Conf. Ser. 660 012005

(<http://iopscience.iop.org/1742-6596/660/1/012005>)

View [the table of contents for this issue](#), or go to the [journal homepage](#) for more

Download details:

IP Address: 141.52.96.106

This content was downloaded on 29/03/2016 at 10:02

Please note that [terms and conditions apply](#).

# Hybrid electromagnetic and electrostatic micromachined suspension with adjustable dynamics

K Poletkin<sup>1</sup>, Z Lu<sup>1</sup>, U Wallrabe<sup>1</sup> and V Badilita<sup>2</sup>

<sup>1</sup> Laboratory for Microactuators, Department of Microsystems Engineering - IMTEK, University of Freiburg, Freiburg im Breisgau D-79110, Germany

<sup>2</sup> Institute of Microstructure Technology, Karlsruhe Institute of Technology, Eggenstein-Leopoldshafen D-76344, Germany

E-mail: vlad.badilita@kit.edu, k.poletkin@gmail.com

**Abstract.** This paper introduces a novel design for a hybrid micromachined contactless suspension, whose operation is based on combining electromagnetic inductive and electrostatic actuation. Wirebonded microcoils provide the electromagnetic inductive actuation, while electrodes patterned on a Si wafer provide electrostatic control. The coil structure and the electrode structure are independently designed and fabricated, and are finally assembled into one device by flip-chip bonding. We demonstrate vertical linear positioning of an aluminium disk-shaped proof mass in a range from 30 to 200  $\mu\text{m}$  based on the coil structure. The electrode structure is employed to dynamically adjust the stiffness components during the operation of the suspension, to control the tilting in a range from  $\pm 1^\circ$  to  $\pm 4^\circ$ , as well as to control the oscillation about the vertical axis with a displacement of  $37^\circ$  at about 1.5 Hz frequency.

## 1. Introduction

This work is continuing the research efforts in our group in the field of micromachined inductive suspensions [1–3] and relates to a more general interest in the micro-engineering community to develop miniaturised actuators such as micro-gyroscopes and micro-motors, by completely eliminating the physical contact between the moving parts of these devices. Many of these devices where the technological solution involves some sort of mechanical contact such as spring structures, hinges, ball bearings, face a series of drawbacks: limited displacements, decrease in sensitivity or in the delivered output force. In order to overcome these limitations, levitation has been employed as a solution to eliminate mechanical contact, therefore to completely eliminate friction and wear in miniaturised sensors and actuators in a series of applications such as as micro-inertial sensors [4–7], frictionless micro-bearings [1, 8], bistable switches [9], micro-accelerator [10], linear-micro-actuator [11], and nano-force sensor [12].

Moreover, the combination of electromagnetics and electrostatics opens new avenues in terms of device capabilities and performance. If levitation and rotation of micro-objects have been demonstrated in a relative straightforward manner only exploiting electromagnetic levitation, by integrating electrodes for electrostatic actuation in the same device, Kraft et al. [10] have achieved an additional feature, i.e., accelerating micro-objects along a predefined path. Improved energy performance of a contactless suspension based on combining diamagnetic and inductive principles has been demonstrated as opposed to employing diamagnetic or inductive suspension separately [13].



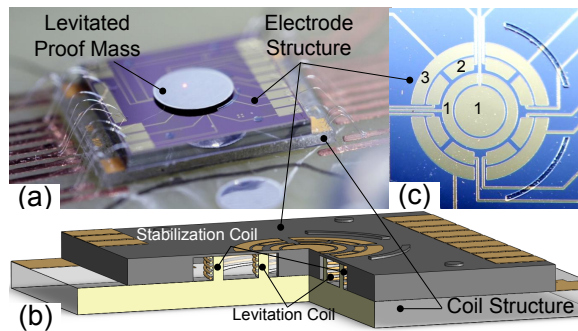


**Figure 1.** The hybrid suspension: a) fully assembled device with the Al proof mass during operation; b) 3D schematic of the device identifying the coil and the electrode structure; c) top view of the electrode structure identifying each set of electrodes: 1-suspending, 2-rotating and 3-tilting electrodes.

We have previously reported micromachined inductive suspensions based on electromagnetic levitation using 3D microcoils obtained by means of an automatic wirebonder. We have extensively characterised the performance of these suspensions [2] and we have developed an analytical model to predict the behaviour as a function of design parameters and input values [1]. In this work, in addition to electromagnetic induction, we employ electrostatics by integrating a series of electrodes in the suspension structure in order to have direct control on the stiffness components of the device. Significantly increased operational capabilities, i.e., linear and angular positioning with adjustable dynamics is also demonstrated herewith.

## 2. The hybrid suspension

### 2.1. Design and fabrication

The device reported here combines electromagnetic induction and electrostatic actuation and a comprehensive visual description is given in Figure 1. For each actuation principle a dedicated structure is designed, namely a coil structure for electromagnetic induction actuation, and an electrode structure for the electrostatic actuation. The coil structure is similar to those reported previously [14] and consists of two coaxial solenoidal microcoils obtained by automatic wirebonding. These coils are wound around  $450\ \mu\text{m}$  tall SU-8 structures defined by UV photolithography. Electrical contacting of the coils is realised via CrAu pads defined on the Pyrex substrate by metallisation, UV patterning and wet etching. In this work the diameters of the two coils are:  $2000\ \mu\text{m}$  and  $3800\ \mu\text{m}$ . As explained in the next section, the role of the inner coil is to provide levitation of the proof mass, while the role of the outer coil is to provide stabilisation of the proof mass during the levitation. In this work the inner (levitation) coil has 20 windings and the outer (stabilisation) coil has 12 windings. The wire used here is  $25\ \mu\text{m}$  insulated gold wire.

The electrode structure is fabricated on a Si wafer by sputtering CrAu (20/150nm), followed by UV photolithography and wet etching. Subsequently, the substrate wafer is etched by deep reactive ion etching (DRIE) from the backside in order to accommodate the coil structure. In the final stage, the electrodes are supported by a silicon membrane with a thickness of  $40\ \mu\text{m}$ . The function of these electrodes is to control the vertical and angular actuation of the proof mass.

In the final fabrication step the electrode structure is mounted on top of the coil structure and the final device is assembled by flip-chip bonding having the following dimensions:  $9.4\ \text{mm} \times 7.4\ \text{mm} \times 1\ \text{mm}$ . For this work we have used a disk-shaped aluminium proof mass with a diameter of  $3.2\ \text{mm}$ . Throughout this work we will refer to the very recent results obtained with a disk-shaped aluminium proof mass with a diameter of  $2.8\ \text{mm}$  [3] and we will place both data sets in the context of the theoretical model developed and reported in [1]. In this way we demonstrate that the experimental data is confirming our theoretically-generated stability map presented in [1].

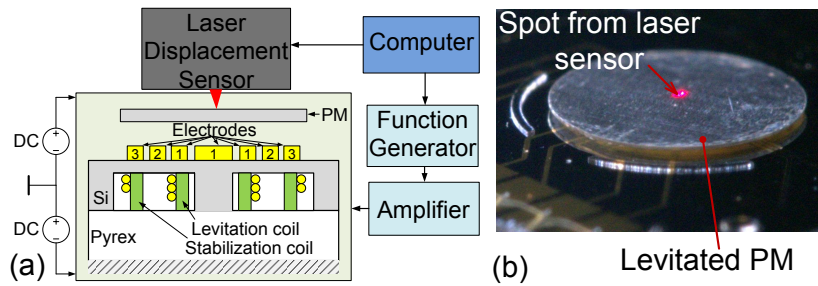


**Figure 2.** The experimental setup: a) schematic and measurement chain; b) Snapshot of the levitating proof mass during the experiment.

## 2.2. Operation of the device

The two coaxial solenoidal coils are biased through a current amplifier (LCF A093R) with square wave AC signals having a phase-shift of  $180^\circ$ , thus providing stable levitation of a circular conductive proof mass. The typical rms current values used in this paper range between 100 and 130 mA for a frequency of 9 MHz, whereas the levitation height varies from 30 to  $180 \mu\text{m}$ , having the top of the electrode structure as reference. A function generator (Arbstudio 1104D) was used to modulate the amplitude and the frequency of the coil currents. A schematic of the experimental setup together with the measurement chain is presented in Figure 2.

The ensemble of the electrode structure fulfils several functions: modulates the vertical actuation, controls the tilting about two horizontal axes, as well as the oscillation about the vertical axis. When central electrodes (“1” - in Figure 1c and Figure 2a) are energised, the levitation height and the dynamics of the proof mass are modulated while maintaining the same amount of current in the coils. The set of electrodes “2” operate according to the variable capacitance principle and determine the angular oscillation of the proof mass when a voltage is applied. We control the tilt of the proof mass with respect to two orthogonal axis in the horizontal plane by biasing the set of electrodes “3”.

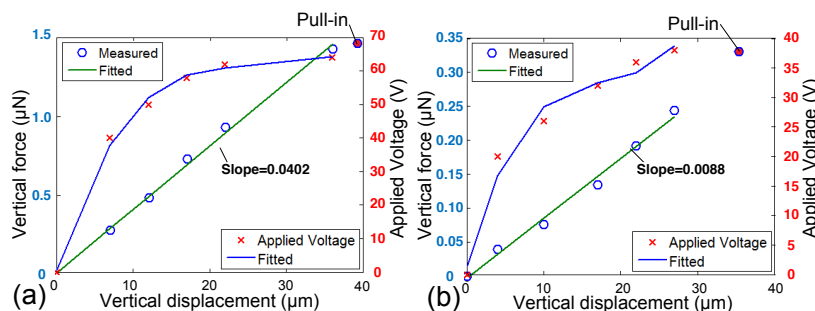
A laser distance sensor (LK-G32) with a resolution of 10 nm was used to measure the linear displacements of the proof mass. The red dot visible in Figure 2b represents the spot from the laser distance sensor.

## 3. Interpretation of experimental results

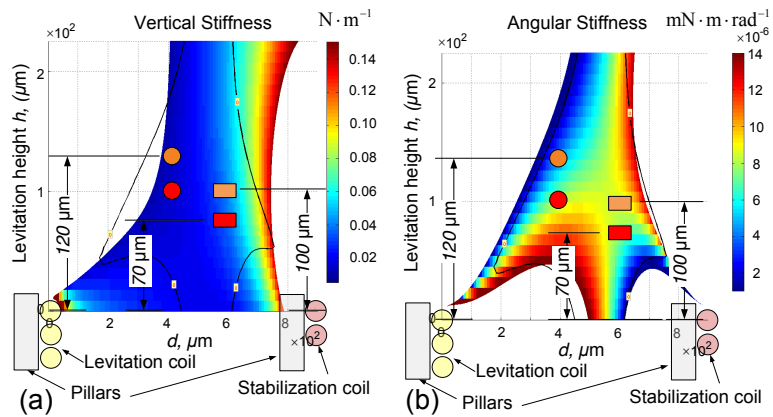
The dynamics of the suspension is governed by the stiffness components. For a complete characterisation of the suspension capabilities, the stiffness components must be measured. To this end, the linear displacements have been recorded simultaneous with the voltages applied on the respective electrodes.

Figure 3a shows the vertical displacement of the proof mass as a function of the applied voltage, along with the vertical force. The electrostatic force between two plates that are oppositely charged is given by the product between the field produced by one of the plates and the charge on the other. In terms of actual physical dimensions and applied voltage, the electrostatic force is given by:

$$F = \epsilon_0 \epsilon_r \cdot \frac{A}{4} \cdot \frac{V^2}{h^2} \quad (1)$$



**Figure 3.** Experimental linear displacements and voltage values for the evaluation of stiffness components: (a) for central electrodes “1”; (b) for outer electrodes “3”.



**Figure 4.** Mapping of the distribution of stiffness components within the stability domain (according to the model in [1]): (a) vertical stiffness; (b) angular stiffness. Circular/rectangular marks correspond to the proof mass with 2.8/3.2 mm diameter. Red/orange corresponds to the case when electrodes “1” are biased/not biased.

where the free space electrical permittivity is  $\epsilon_0$ , the relative permittivity for air is  $\epsilon_r$ ,  $V$  is the applied voltage,  $A$  is the overlapping area between the electrodes and the proof mass and  $h$  is the distance between the plates, in this case the vertical displacement given in Figure 3. The value for the overlapping area  $A$  for electrodes “1” is  $8.0 \cdot 10^{-7} m^2$ , and for electrodes “3” is  $4.3 \cdot 10^{-7} m^2$ . The measurements presented in Figure 3, combined with the analytical model developed and presented in [1] yield the values for the vertical and angular stiffness components, which are included in Table I, column I, for the proof mass with a diameter of 3.2 mm used in this paper. As predicted by the theoretical model [1], we observe a consistent increase in stiffness compared to the experimental values reported in [3] when using a smaller proof mass, with a diameter of 2.8 mm.

In Figure 4 we provide a contextual overview by consolidating the experimental results obtained in this work using a proof mass with 3.2 mm diameter, as well as the results reported previously [3] using a lighter proof mass with 2.8 mm diameter, on the same map of stiffness components elaborated using our analytical model presented in [1]. Integrating the electrode structure offers the possibility to modulate the vertical positioning of the proof mass not only by changing the current in the coils, but also by applying a voltage to the electrodes, in this

**Table 1.** Measurement and modelling.

	Proof mass	3.2 mm	Proof mass	2.8 mm *
Measurement no.	I	II	III	IV
Measured stiffness				
Angular, [ $Nm \cdot rad^{-1}$ ]	$1.1 \cdot 10^{-8}$	$0.7 \cdot 10^{-8}$	$0.6 \cdot 10^{-8}$	$2.1 \cdot 10^{-8}$
Vertical, [ $N \cdot m^{-1}$ ]	0.040	0.040	0.026	0.026
Modelled stiffness**				
Angular, [ $Nm \cdot rad^{-1}$ ]	$0.8 \cdot 10^{-8}$	$0.5 \cdot 10^{-8}$	$0.4 \cdot 10^{-8}$	$0.9 \cdot 10^{-8}$
Vertical, [ $N \cdot m^{-1}$ ]	0.042	0.042	0.024	0.024
Parameters				
Levitation height, [ $\mu m$ ]	100	70	120	100
Voltage on electrodes “1”, [V]	0	54	0	42
Coil current, [mA]	115	115	115	115

\* reported in [3]

\*\* developed in [1]

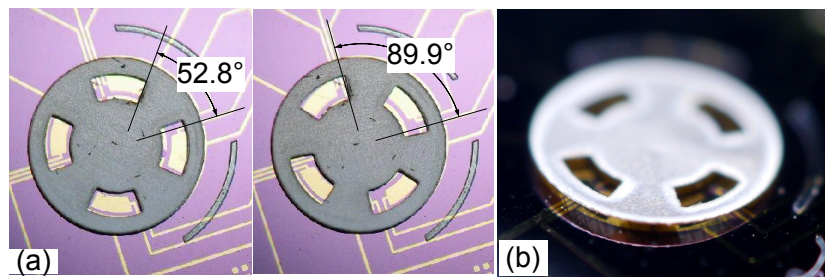


**Figure 5.** a) Angular oscillation in the horizontal plane around the vertical axis; b) Snapshot of the levitated carved proof mass executing the oscillations.

case the electrodes labeled “1”. Using the electrostatic force generated while applying a voltage on electrodes “1”, the proof mass can be maintained at a certain height even when the current in the levitation coil is increased, therefore changing the angular stiffness of the respective proof mass. This is demonstrated by applying a voltage of 54 V on electrodes “1” and recording a levitation height of 70  $\mu\text{m}$ , as opposed to 100  $\mu\text{m}$  for the same current in the coil structure, but no voltage applied to the electrodes.

The analytical model presented in [1] predicts a very slight change in the vertical stiffness when electrodes “1” are biased and the current in the coils is maintained constant. This is confirmed by the experimental results obtained here, as well as in [3], and reported in Table I: the vertical stiffness components both with and without applying the additional electrostatic force are  $0.040 \text{ N} \cdot \text{m}^{-1}$  and  $0.026 \text{ N} \cdot \text{m}^{-1}$  for the 3.2 mm and 2.8 mm diameter proof mass, respectively. The analytical model also predicts that the variation of the angular stiffness depends on the diameter of the proof mass. For the 2.8 mm diameter proof mass the angular stiffness increases upon biasing electrodes “1” ( $0.9 \cdot 10^{-8}$  versus  $0.4 \cdot 10^{-8} \text{ Nm} \cdot \text{rad}^{-1}$ ), whereas for the 3.2 mm diameter proof mass the angular stiffness decreases upon biasing electrodes “1” ( $0.5 \cdot 10^{-8}$  versus  $0.8 \cdot 10^{-8} \text{ Nm} \cdot \text{rad}^{-1}$ ). This excellent agreement between the theoretical predictions and the experiment is synthetically presented in Figure 4.

Figure 5 shows the operation of the device upon biasing electrodes “2” with a voltage of  $\pm 10\text{V}$ , thus creating two phases. The proof mass oscillates with  $37^\circ$  amplitude at 1.5 Hz frequency.

#### 4. Conclusion

This work consolidates our studies on inductive suspensions and together with the results reported recently [3] confirms the predictions of our linear analytical model presented in [1].

#### Acknowledgments

KP acknowledges support of the Alexander von Humboldt Foundation (Grant RUS-1149346 STP). VB acknowledges support from German Research Foundation (Grant BA 4275/2-1).

#### References

- [1] Lu Z, Poletkin K, den Hartogh B, Wallrabe U and Badilita V 2014 *Sensor. Actuat. A-Phys.* **220** 134–143
- [2] Lu Z, Poletkin K, Wallrabe U and Badilita V 2014 *Micromachines* **5** 1469–1484 ISSN 2072-666X
- [3] Poletkin K, Lu Z, Wallrabe U and Badilita V 2015 *Microelectromechanical Systems, Journal of* **in Press** DOI: 10.1109/JMEMS.2015.2469211
- [4] Han F, Sun B, Li L and Wu Q 2015 *IEEE Sensors J.* **15** 209 – 217
- [5] Su Y, Xiao Z, Ye Z and Takahata K 2015 *IEEE Electron Device Lett.* **36** 393–395
- [6] Nakamura S 2005 MEMS inertial sensor toward higher accuracy & multi-axis sensing *Proc. 4th IEEE Conf. Sensors* pp 939–942
- [7] Shearwood C, Ho K, Williams C and Gong H 2000 *Sensor. Actuat. A-Phys.* **83** 85–92
- [8] Coombs T, Samad I, Ruiz-Alonso D and Tadinada K 2005 *IEEE Trans. Appl. Supercond.* **15** 2312–2315
- [9] Dieppedale C, Desloges B, Rostaing H, Delamare J, Cugat O and Meunier-Carus J 2004 Magnetic bistable micro-actuator with integrated permanent magnets *Proc. IEEE Sensors* vol 1 pp 493–496
- [10] Sari I and Kraft M 2015 *Sensor. Actuat. A-Phys.* **222** 15–23
- [11] Ruffert C, Gehrking R, Ponick B and Gatzten H H 2006 *IEEE Trans. Magn.* **42** 3785–3787
- [12] Abadie J, Piat E, Oster S and Boukallel M 2012 *Sensor. Actuat. A-Phys.* **173** 227–237
- [13] Liu K, Zhang W, Liu W, Chen W, Li K, Cui F and Li S 2010 *Microsyst. Technol.* **16** 431–439
- [14] Lu Z, Jia F, Korvink J, Wallrabe U and Badilita V 2012 Design optimization of an electromagnetic microlevitation system based on copper wirebonded coils *2012 Power MEMS* (Atlanta, GA, USA) pp 363 – 366